The strong SDA/framework interactions and acidity study of high-silica LTA-type zeolites

Haimei Xu, Peng Lu, Guangying Fu, Jifa Miao, Jiaqi Zhao, Ruiqin Ding, Lei Zhao, Zhirong Lang, Xiaobo Yang, Valentin Valtchev

The strong SDA/Framework Interactions and Acidity Study of High-silica LTA-type zeolites

Haimei Xu,[a] Peng Lu,[a] Guangying Fu,[a] Jifa Miao,[a] Jiaqi Zhao,[a,b] Ruiqin Ding,[a] Lei Zhao,[a] Zhirong Lang,[a] Xiaobo Yang,*[a] Valentin Valtchev*[a,c]

[a] The ZeoMat Group, Qingdao Institute of Bioenergy and Bioprocess Technology, Chinese Academy of Science, Laoshan District, CN-266101 Qingdao, China.

E-mail: yangxb@qibebt.ac.cn

[b] College of Chemical Engineering, China University of Petroleum (East China), CN-266580 Qingdao, China

[c] Normandie University, ENSICAEN, UNICAEN, CNRS, Laboratoire Catalyse et Spectrochimie, F-14000 Caen, France.

E-mail: valtchev@ensicaen.fr

Abstract

The zeolite community spent 50 years in pursuing the synthesis of high-silica **LTA**-type zeolites, and ultimately succeeded with the pure-silica polymorph by applying specific structure-directing agents (SDA). The high-silica zeolite A has exhibited unique properties and strong potential to be applied as an adsorbent and catalyst in several novel processes. In the present study, the high-silica polymorphs of Si/Al ratios from 15 to ∞ were synthesized and subjected to thorough characterizations using multiple physicochemical methods. It has been revealed that there exists strong interactions between the organic SDAs and the framework. Therefore, removing the SDAs by calcination in air is difficult, and can only be done above 700 ^{o}C with a certain degree of framework dealumination. The retained framework structure shows connectivity defects and a unique combination of Brønsted and Lewis acidity. Using methanol-to-olefins (MTO) as a probe reaction, the catalytic performance of high-silica **LTA**-type zeolites has been evaluated. Compared to the well-studied **CHA** and **MFI**-type catalysts, high-silica zeolite A exhibited a shorter life-time and higher selectivity towards C_4 olefins, while methane selectivity increased with the deactivation.

KEYWORDS: zeolite; Si-rich **LTA**-type zeolites; MTO; acidity; catalyst design

1. Introduction

Linde Type Zeolite A (topology type code **LTA**) is among the first synthetic zeolites that have been commercialized since 1950s. It is used in various applications as an adsorbent in solvent desiccation, air separation, air conditioning, remote oxygen generation for medical uses, as ion-exchanger in detergents, and in many others that cover almost all industrial and domestic sectors.[1-3] The latest estimate of the market size for zeolite 4A in 2022 was USD 1302.19 million, and is forecasted rising to USD 1614.03 million by 2028.[4] Zeolite A is usually synthesized from highly alkaline mixtures of silicates and aluminates, which results in a material with an almost strict chemical formula $|Na^+, x\ H_2O|[SiAlO_4]$-**LTA**, i.e., the framework Si/Al = 1, a value at the lowest limit of Löwenstein's rule.[5, 6] The framework of **LTA** is built of $[4^6 6^8]$ sodalite-cages (*sod*) connected through *d4r* cubes, forming then a big $[4^8 6^8 8^6]$ cage (*lta*), which is accessible for diffusing gas molecules through the 8-ring windows. Na^+ ions in the cages are exchangeable by other cations such as K^+, Ca^{2+}, etc. And the ion-exchanged zeolite A materials exhibit slightly modified diameters for effective diffusion paths. The K-, Na- and Ca-forms of zeolite A are known as 3A, 4A and 5A, which implies that these zeolites have diffusion passages of around 3, 4 and 5 Å in diameter.[1, 7] However, the proton-exchanged form of the low framework Si/Al ratio would collapse upon heating. Therefore it cannot be applied as a solid-acid catalyst, while the acidity related catalytic activities are major applications of many other zeolites.[8-12] Therefore, attempts to raise the Si/Al ratio of **LTA**-type zeolites in the

synthesis have been carried out but have proven to be a challenging task for many decades. In 1960s, a number of **LTA**-type zeolites of higher Si/Al ratios up to *ca.* 3 were synthesized using tetramethylammonium ion as an organic structure-directing agent (SDA).[13-16] In 2004, by employing a combination of tetramethylammonium (TMA^+) and tetraethylammonium (TEA^+) cations, the framework Si/Al ratio was further raised to *ca.* 5.[17] The high-silica **LTA**-type zeolite showed a certain activity in the catalytic conversion of methanol-to-olefins (MTO).[18] The significant breakthrough was achieved in 2004 with the successful synthesis of a material named ITQ-29 by Corma et al,[19] where Al-free ITQ-29 was prepared in F^- media using a π−π stacking supramolecular complex of methylated julolidine as the SDA with an addition of Ge (Si/Ge = 2). Introducing Ge into the gel to work in F^- media helps to link the sodalite cages forming the corresponding *d4r* units, which directs the formation towards LTA structure instead of the sodalite. These authors were able to finally raise the Si/Al ratio of **LTA**-type zeolites from T(IV)/T(Ⅲ) = 13 to infinity using a combination of this supramolecular complex and TMA^+ as the SDAs.[19, 20] The Al-free version of ITQ-29 was proven to be an inert adsorbent for hydrocarbon separations preventing oligomerization side-effects, while the aluminosilicate ITQ-29 of T(IV)/Al = 20 was an able shape-selective catalyst as an FCC additive for boosting olefin yields.[19] Another advantage of pure-silica ITQ-29 is the extreme thermal stability that resists 900 ^oC calcination without the structural collapse that would occur to the aluminum-rich zeolite A. In 2015 another organic SDA, an quaternary imidazolium mono-compound found by Zones and Davis was able to facilitate the crystallization of

pure-silica and high-silica **LTA**-type zeolites in the fluoride medium.[7] The aluminosilicate zeolites of Si/Al = 12 to 42 exhibited a unique MTO activity, yielding more C_4-C_6 products than **CHA**-type zeolites such as SAPO-34 and SSZ-13, which are frequently applied for MTO reactions and yield more C_2 and C_3 olefins.[7] Later, it was also demonstrated that Cu^{2+}-exchanged high-silica **LTA** zeolite (Si/Al = 16) was active in selective catalytic reduction (SCR) of NOx emissions of Diesel exhausts, which is again a benchmark application of SSZ-13.[21]

Thus, the 50-year challenge towards the pure-silica **LTA**-type zeolite has been solved by the discoveries of specific SDAs. The obtained pure-silica and high-silica materials exhibit unprecedented catalytic properties. In the present paper, we take the imidazolium-synthesized **LTA**-type high-silica zeolites as objects, elucidate the SDA/framework interactions with experimental results, and thoroughly characterize the acidity of the materials after the removal of the SDA. We use MTO as a probe reaction to discuss the catalytic behaviors of obtained materials with the unique acidity.

2. Experimental section

2.1 Synthesis

2.1.1 SDAs:

1,2-dimethyl-3-(4-methylbenzyl)imidazolium hydroxide $[(1,2\text{-DM-3-(4-MB)I}]^+OH^-$, ROH) was used as an organic structure-directing agent (SDA), together with

trimethylammonium hydroxide (TMAOH), for the zeolite synthesis in the present study. ROH was prepared according the literature procedure.[7, 21] A mixture of 0.1 mol 1,2-dimethylimidazole (98%) and 0.1 mol 4-methylbenzyl chloride (98%, TCl) was refluxed in 100 mL toluene (99.8%) at 110 ^{o}C for 2 days. Then, it was cooled to 25 °C. The resulting solids were filtered and washed by ethyl-ether (99%). The obtained white solid had ^{1}H NMR (300 MHz, D_2O) signal at δ =7.22-7.07, 5.16, 3.64, 2.44, 2.21 ppm.

The R-iodide salt was then converted to the hydroxide form using a strongly basic ion-exchange resin (Dowex Marathon A, hydroxide form) in water. The product was titrated using 0.0105 M HCl.

2.1.2 Synthesis of the pure-silica LTA-type zeolite

The composition of the synthesis gel was 0.45 ROH: 0.05 TMAOH: 0.5 HF: 1.0 SiO_2: 5 H_2O, R stands for 1,2-DM-3-(4MB)I.[7, 21] It was prepared by stirring ROH, tetramethylammonium hydroxide pentahydrate (TMAOH·5H_2O, 97 %), and tetraethylorthosilicate (TEOS, 98 %) at 25 °C until TEOS hydrolyzed. Heating the resulting mixture at 40 °C was to remove ethanol generated by TEOS hydrolysis as well as excess water. Hydrofluoric acid (HF, 40 %) was then added dropwise to the gel. The thick gel was quickly mixed with a spatula. The mixture was charged into Teflon-lined 23-mL autoclaves and heated under rotation (15 rpm) at 170 °C for 4 days. The solid product was successively washed with DI H_2O (3 × 10 mL) and acetone/methanol (1:1, 3 × 10 mL), dried overnight at room temperature. Calcination

was performed in air at 250 ºC for 6 h and 720 ºC for 6 h to remove the SDAs.

2.1.3 Synthesis of LTA-type zeolites with Si/Al = 15-100

Aluminum isopropoxide (99.9 %) was added as the aluminum source to the above recipe in the synthesis of high-silica **LTA**-type zeolites. A small amount of the calcined pure-silica material was used as seeds (4 wt% on the silica basis in the synthesis mixture). The composition of the synthesis mixtures were 0.5 ROH: x TMAOH: 0.5 HF: 1.0 SiO_2: 0.5x Al_2O_3: 5 H_2O, where $x = 0.01 \leq x \leq 0.067$.

2.2 Characterization

Powder X-ray diffraction (XRD) patterns were collected using a Rigaku LabView diffractometer in the 2Theta range of 5 to 50^o with 0.01^o scan steps in the theta-theta geometry under Cu Kα-radiation. Thermogravimetric and Differential Thermal Analysis (TG/DTA) was carried out on a Rigaku TG-DTA8122 thermal analyzer system in 50 mL/min air flow with a heating rate of 10 °C/min from 30 to 900 °C. Scanning electron microscopy (SEM) was operated on a Hitachi S-4800 microscope equipped with a cold field emission gun operated at 1–5 kV. Argon (Ar) physisorption isotherms were measured on a Quantachrome Autosorb iQ at 87 K. Before the measurements, the samples were degassed at 300 ^oC under vacuum for 10 h. Temperature-programmed desorption of ammonia (NH_3-TPD) was carried out in a flow system with a thermal conductivity detector (TCD). Using deuterated acetonitrile (CD_3CN) as a probe molecule, Fourier transform infrared spectroscopy (FTIR) was

performed on Brucker Vertex 70 V Spectrometer at a spectral resolution of 4 cm^{-1}. In a home-made vacuum infrared cell with CaF_2 windows, a self-supported wafer of the sample (about 10 mg/cm^2) was initially dried under vacuum at 450 ^oC for 2 h and then cooled down to 25 ^oC. A reference spectrum was recorded. Afterwards, the wafer was saturated with CD_3CN vapor at 25 ^oC for 10 min and then evacuated again for 30 min to remove CD_3CN in the gas phase. Finally, the evacuated sample containing chemisorbed CD_3CN was subjected to temperature-programmed desorption at 150, 250, 350 and 450 ^oC for 30 min at each temperature with a heating rate of 10 ^oC /min. FTIR spectra were recorded after cooling down to 25 ^oC. ^{29}Si and ^{27}Al MAS NMR experiments were performed on Bruker AVANCE III 600 spectrometer with a 4 mm triple resonance probe operating at a resonance frequency of 156.4 MHz and 119.2 MHz, respectively. ^{29}Si MAS NMR spectra with high-power proton decoupling were recorded with a spinning rate of 10 kHz, a $\pi/4$ pulse length of 2.9 μs, and a recycle delay of 20 s. ^{27}Al MAS NMR spectra were recorded using a small-flip angle technique with a pulse length of 0.5 μs ($<\pi/12$),a 1s recycle delay and a spinning rate of 14 kHz. The chemical shifts of ^{27}Al and ^{29}Si MAS were referenced to 1 mol/L aqueous $Al(NO_3)_3$ and Tetramethylsilane (TMS), respectively. ^{19}F MAS NMR was carried out on Bruker AVANCE III 600 spectrometer at a resonance frequency of 564.5 MHz using a 4 mm HX double-resonance MAS probe at a spinning rate of 15 kHz. ^{19}F MAS NMR spectra were recorded with a $\pi/2$ pulse length of 3.5 μs and a 10 s recycle delay. The chemical shifts were referenced to trichlorofluoromethane ($CFCl_3$).

2.3 Catalytic test

Catalytic tests were performed using a fixed-bed tubular micro-reactor, with 5.0 mm inner diameter at 400 ^{o}C. 450 mg catalysts (150-300 μm) were charged. Methanol has been fed by saturation of 30 ml/min of N_2 by 0.005 ml/min of methanol, thus giving a weight hourly space velocity (WHSV) of 2 h^{-1}. The product stream was analyzed with a gas chromatograph (GC) equipped with FID detector and automatic sampling (Plot-Q column).

Product selectivity was defined as the mole ratio of each product (on C1 basis) referred to moles of converted methanol. The following products were detected during the reaction: methane, light olefins (ethylene, propylene and butenes) and C_2-C_4 alkanes, and higher hydrocarbons (C_5^+).

3. Results and Discussion

3.1 The synthesized LTA-type zeolites with Si/Al = 15 - ∞

The synthesis method was adapted from the literature.[7, 21] As shown in Table 1, the Si/Al ratios of the initial gel were ∞, 100, 50, 25 and 15. The recovered solid products out of these recipes were denoted as LTA-*n*, with *n* representing the corresponding initial gel Si/Al ratio. The XRD patterns in Figure 1(a) show that all 5 samples of the as-synthesized LTA-*n* are phase-pure and highly crystalline zeolites of the **LTA**-type.

Table 1. The synthetic recipes, hydrothermal conditions, and the Si/Al ratios of the products analyzed by XRF and solid-state NMR.

Name	Initial gel composition						Conditions		Si/Al ratio		
	ROH	TMAOH	Si	Al	H_2O	HF	T (°C)	t (d)	XRF	NMR^1	NMR^2
LTA-∞	0.45	0.05	1	0	5	0.5	170	4	∞	∞	∞
LTA-100	0.5	0.01	1	0.01	5	0.5	170	4	68	79	84
LTA-50	0.5	0.02	1	0.02	5	0.5	170	4	41	31	34
LTA-25	0.5	0.04	1	0.04	5	0.5	170	4	25	17	24
LTA-15	0.5	0.067	1	0.067	5	0.5	170	4	14	10	16

ROH: 1,2-dimethyl-3-(4-methylbenzyl)imidazolium hydroxide.

TMAOH：Tetramethylammonium hydroxide.

XRF: Si/Al ratio detected by XRF of as-synthesized LTA zeolites.

NMR^1: The framework Si/Al ratio was calculated by ^{29}Si MAS NMR of as-synthesized LTA zeolites.

NMR^2: The framework Si/Al ratio was calculated by ^{29}Si MAS NMR of calcined LTA zeolites.

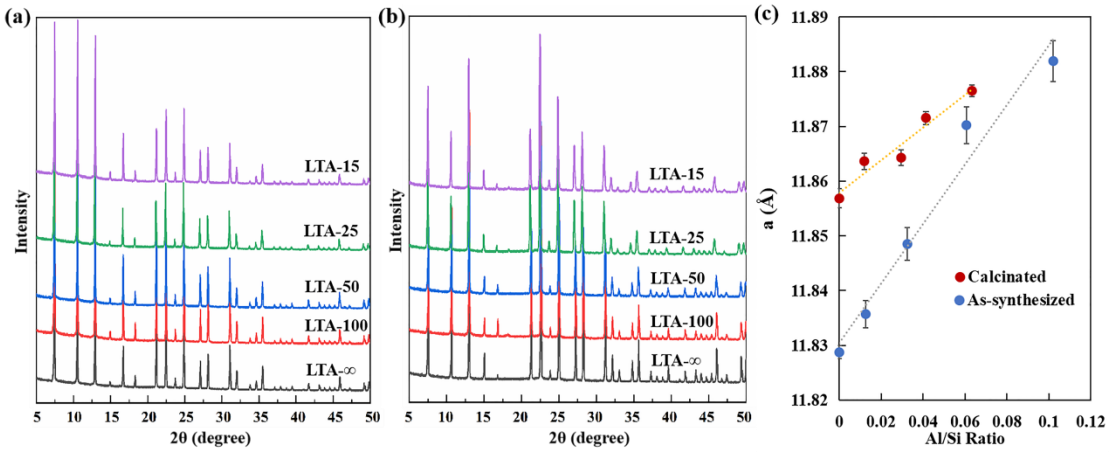

Figure 1. Powder XRD as-synthesized (a) and calcined (b) LTA-*n* zeolites. (c) Refined unit cell parameters *a* in the cubic unit cell for both sample series as a function of

framework Al/Si ratios.

The SEM images of the materials (Figure 2) show pure and well-shaped crystals. They are all cubic, occasionally showing also truncated edges and corners beside the (100) faces which are typical for **LTA**-type zeolites. Since these crystals had crystallized from condensed thick gels with H_2O/SiO_2 = 5, where nucleation occurred in a not-controlled manner, the sizes of the crystals seem random. But in general, the aluminosilicate versions have smaller sizes than the pure-silica sample because of favored nucleation occurring in the aluminum-containing gels. The pure-silica crystals are close to 8 μm large; the aluminosilicates have smaller sizes, specifically, around 5 μm for LTA-100, 6 μm for LTA-50, 1 μm for LTA-25, and 3 μm for LTA-15. The crystal sizes do not show an obvious dependency on the synthesis recipes for the high-silica products.

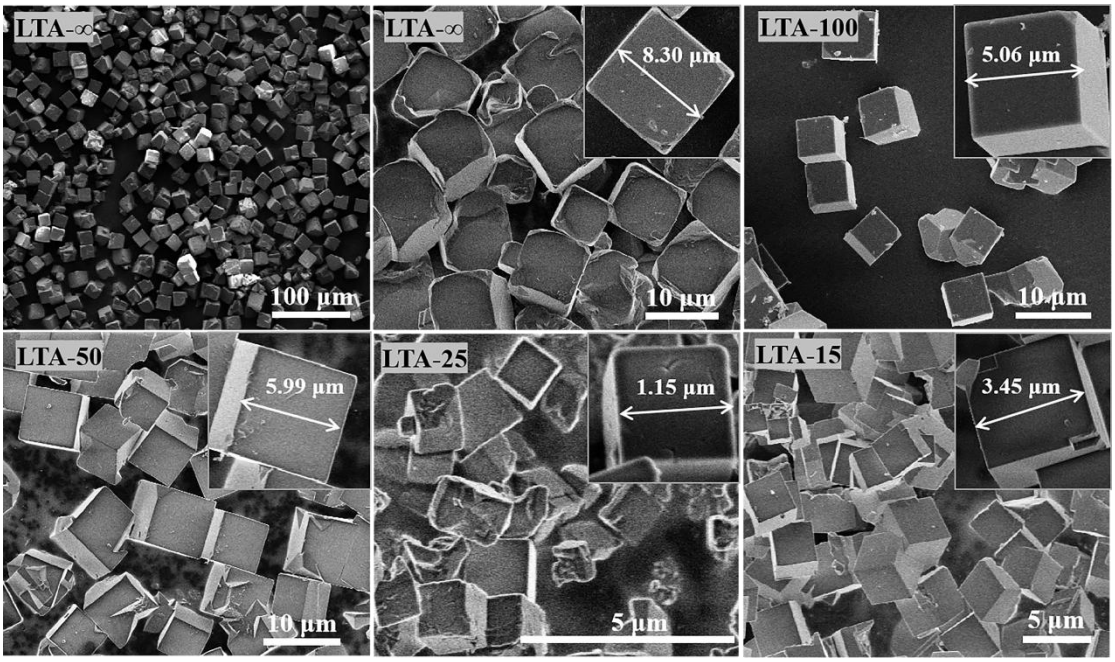

Figure 2. SEM images of as-synthesized LTA-*n* zeolites.

The Si/Al ratios of the as-synthesized materials were determined with XRF and ^{29}Si MAS NMR (Table 1). The XRF results of as-synthesized samples reflex the global compositions of the solid, while the NMR results represent the ratios of the framework T atoms. Albeit the larger error scales of the XRF method, there is an observable tendency regarding the incorporation of Al atoms in the products, i.e., the products have higher Al ratios than the initial gel provided. This phenomenon frequently happens in zeolite synthesis due to the different solubility of silicate and aluminate species.

Figure 1(c) shows that the unit cell length *a* (cubic unit cell in the space group *Pm-3m* #221) increases rapidly with the framework Al/Si ratio for the as-synthesized LTA-*n* materials. The bigger error bars in the refined *a*-values imply bigger gaps between the real material and the ideal lattice, i.e., the structural distortions. SiO_4-tetrahedron is a rather rigid framework-building unit that can only assume conformations strictly around the ideal tetrahedron with Si-O length at 1.6 Å and O-Si-O angle at 109.5°. Conversely, AlO_4-tetrahedron is much more flexible, allowing bigger deformations regarding Al-O length around 1.7 Å, and the O-Al-O angle. Therefore, in the zeolite topologies with remarkable tensions, **LTA** with many *d4r*-units that are unfavorable for a 4-connected framework is one of the cases, the incorporation of Al atoms is favored to release the structural tensions. This also explains, that the synthesis of high-silica **LTA**-type zeolites is challenging, and specific SDAs are required to interact with and force the formation of the silica-framework.

3.2 SDA/framework interaction and SDA removal through calcination

The thermal degradation of the organic template in the zeolite pores depends on several factors, the most important are: the type of structure and the channel system, the interaction between the SDA and the framework, the size of the crystals, and the thermal stability of the molecule. Small pore cage-type zeolites usually release the products of Hofmann degradation at higher temperatures with respect to medium/large pore zeolites with a multi-dimensional channel system. Still, the template degradation of the cage-type zeolites is usually completed up to 500 °C. In the case of high-silica LTA, the template combustion is extended to a much higher temperature over 700 °C, which suggests strong interactions between the SDAs and the framework (Figure S1). There are three observable modules related to the degradation and combustion of SDAs accommodated in the high-silica LTA-*n* materials (Figure S2). In the pure-silica material, an endothermic weight-loss starts at ca. 430 °C and peaks at ca. 466 °C, which could be due to the degradation of SDAs. Following it, there is a sharp heat flow peak at around 555 °C with corresponding to the combustion of two types of SDA cations, TMA^+ and $[1, 2\text{-DM-3-(4-MB)}]^+$ or R^+. Further, the second broader exothermic weight loss at 630 °C may be a summation of the slow combustion of hard decomposition pieces of both SDA ions. The weight losses are completed only at above 700 °C. The total weight loss between 300 and 800 °C counts to *ca.* 26 wt%. The weight-losses for the aluminum-containing LTA materials are similar, but the first combustion step moves towards lower temperatures with increasing Al-contents, while

the separate endothermic decomposition step becomes less announced. The acidity may contribute to the earlier ignition of the organic SDA cations. However, the second combustion step remains at about 630 °C and completes at over 700 °C. Here we are dealing with the removal of two types of SDA cations, TMA^+ and [1, 2-DM-3-(4-MB)]$^+$ or R^+. Since alkaline ions are not present in the recipe, the formation of *sod*-cages requires TMA^+ as the SDA. Thus, there must be TMA^+ occulted in *sod*-cages. Meanwhile, R^+ is too big to reside in *sod*-cage, and must occupy *lta*-cage. Bearlocher and Maier studied the configuration of TMA^+ in *sod* and revealed short contacts between the TMA^+ methyl groups and the framework O atoms and strong C-H···O interaction.[22] Kuehl et al. studied the degradation of TMA^+ in zeolite alpha (**LTA**), and pointed out that *sod*-cage TMA^+ ion decomposes below 465 °C to NH_3, C_2H_2 and CH_4. The former 2 molecules leave the cage through the 6 MR windows, while CH_4 cannot pass the window. It remains in the cage and is converted to olefins, tars, and cokes when the temperature further arises.[23] Fortunately, in high-silica and pure-silica LTA when a point defect occurs at the *sod*-cage, and allows the passage of those hydrocarbons, or the passage of O_2 to burn off them. Especially for the aluminosilicate versions, bridging -OH groups (BAS) pointing in the *sod*-cage may facilitate the ignition of hydrocabons.[24] R^+ molecule in the *lta*-cage may leave following a different route. It has a flexible conformation and may assume various configurations to make itself fitting in the *lta*-cage. However, its bulky shape may hinder the diffusion of O_2 into the cage. When a portion of the initial decomposition products has left and liberate certain spaces for O_2, the combustion

becomes ignited, and the products are liberated through 8 MR windows rapidly. Therefore the combustion temperature is higher than usual zeolites.

The white powders of the LTA-*n* materials, after the static calcination in air at 720 °C retain high crystallinity as shown in the XRD patterns in Figure 1(b). The values of cubic unit cell edge *a* are greater than the as-synthesized counterparts and grow slower with the increase of framework Al contents (Figure 1(c)). The error bars of the *a*-values also become significantly narrower. Without SDAs in the cages, the framework structures become relaxed and less distorted. On the contrary, at the as-synthesized state, the SDAs attract the cage walls inside, making the structure deformed and tighter.

The porosity and specific surface area of the calcined materials have been determined by Ar adsorption at 87 K. Figure S3 shows the obtained isotherms. The isotherms are the classical Type I with a sharp Ar uptake at low relative pressures ($P/P_0 < 0.01$) followed by nearly horizontal adsorption and desorption branches. All samples have similar microspore volumes (V_{mic} by t-plot method) *ca.* 0.24-0.30 cm^3/g (Table 2). Upon calcination, the SDAs have been removed, and the crystalline structure retained; thus, the uniform micropores become available. The BET specific surface areas (S_{BET}) are in the range of 670-780 m^2/g. For Al-contained LTA-*n* zeolites, the highest S_{BET} of LTA-25 (712.4 m^2/g) could be due to the smallest particle size as shown in Figure 2.

Table 2. Textural properties of calcined LTA-*n* zeolites.

Samples	S_{BET} (m^2/g)	S_{ext} [a] (m^2/g)	V_{mic} [b] (cm^3/g)
LTA-∞	772.1	2.9	0.27
LTA-100	630.6	54.1	0.24
LTA-50	647.8	59.6	0.24
LTA-25	712.4	51.3	0.27
LTA-15	660.4	32.9	0.26

[a] The external surface area was determined by t-Plot method.

[b] The micropore volume was obtained by t-Plot method.

Besides the structural relaxation and the release of lattice tensions, the calcination leads, unfortunately, to a negative result, i.e., framework dealumination. In ^{29}Si MAS NMR the main resonances for all as-synthesized and calcined samples appear in the range from -100 ppm to -120 ppm with dominating signals at around -105 and -110 ppm (Figure 3), which are the characteristic peaks of tetrahedral Si species surrounded by three and four SiO_4-tetrahedra (associating to Q^3 Si species, $Si(OSi)_3(OAl)$ and Q^4 Si species, ($-Si(OSi)_4$)) respectively.[1] However, another band at -100 ppm with weak intensity is observed, too, which is attributed to $Si(OSi)_3(OH)$ species, indicating the presence of nest-type silanol defects.[25] The ratios of Q^3 $Si(OSi)_3(OAl)$ species increase with increasing Al portions. The fitted peak areas for individual peaks are given in Table S1 and S2, which are used to calculate the framework Si/Al ratios of the as-synthesized and calcined materials according to the formula.[26]

$$(Si/Al)NMR = \frac{\mathrm{A}(Si(OSi)_4) + \mathrm{A}(Si(OSi)_3(OAl)) + \mathrm{A}(Si(OSi)_3(OH))}{0.25\mathrm{A}(Si(OSi)_3(OAl))}$$

Each A denotes the peak area of the NMR signal of Si(nAl) building unit.

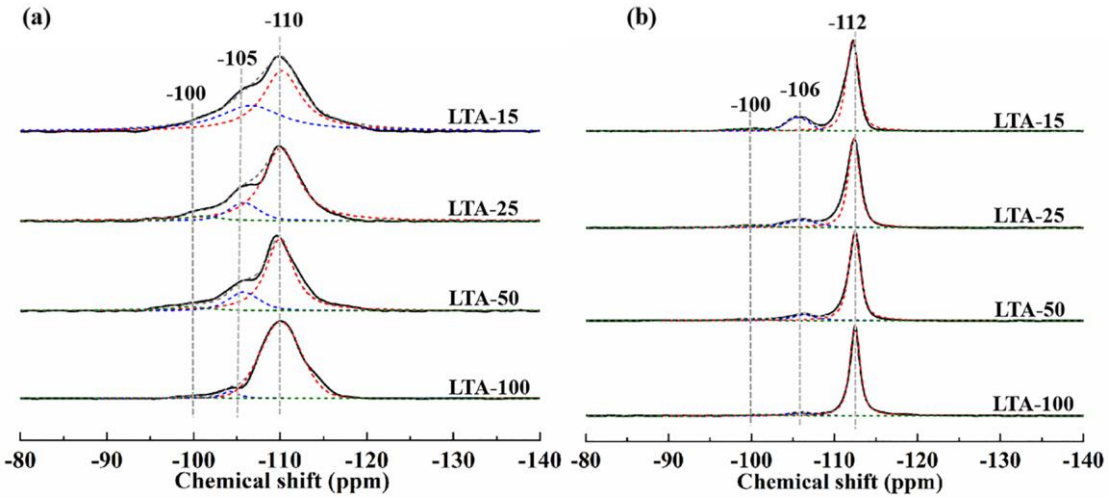

Figure 3. ^{29}Si MAS NMR spectra of the as-synthesized (a) and calcined (b) LTA-*n* zeolites.

The framework Si/Al ratios of calcined samples are higher than the corresponding as-synthesized samples (Table 1) because small amounts of Al leave the framework upon calcination. The ^{29}Si NMR peaks are sharper and better resolved for the calcined than the as-synthezised samples, reflecting more structural tensions and distortions when SDAs exist in the cages. The XRD and ^{29}Si NMR data mutually confirm each other regarding the strong SDA-framework interactions.

^{27}Al MAS NMR spectra of all as-synthesized LTA-*n* samples exhibit solely the resonance at around 58.5 ppm (Figure 4a) of tetra-coordinated framework Al (Al^{IV}). After calcination, the detached Al atoms assume various states of species. The resonances at 1.3 ppm and -7.5 ppm are observed for all samples (Figure 4b),

corresponding to extra-framework hexa-coordinated Al (Al^{VI}).[27] These two peaks could be due to extra-framework Al presented in different forms as hydrated/oxidic cations or neutral species occupying various micropores.[28] In addition, in the high-silica versions for calcined samples, LTA-100, LTA-50, and LTA-25, the resonance at 46.0 and 31.0 ppm are apparent, indicating framework tetrahedral Al sites that are not fully connected and less ordered.[25, 29] Besides, for these samples, the resonance at 31 and/or 17.1 ppm associated with penta-coordinated Al (Al^{V}) are observed as well. This indicates there are connectivity defects in the framework. The concentration of differently coordinated Al calculated based on the area ratio of corresponding peaks was given in Table S3. Among the calcined samples, LTA-15 possesses the highest portion of 4-fold coordinated Al atoms.

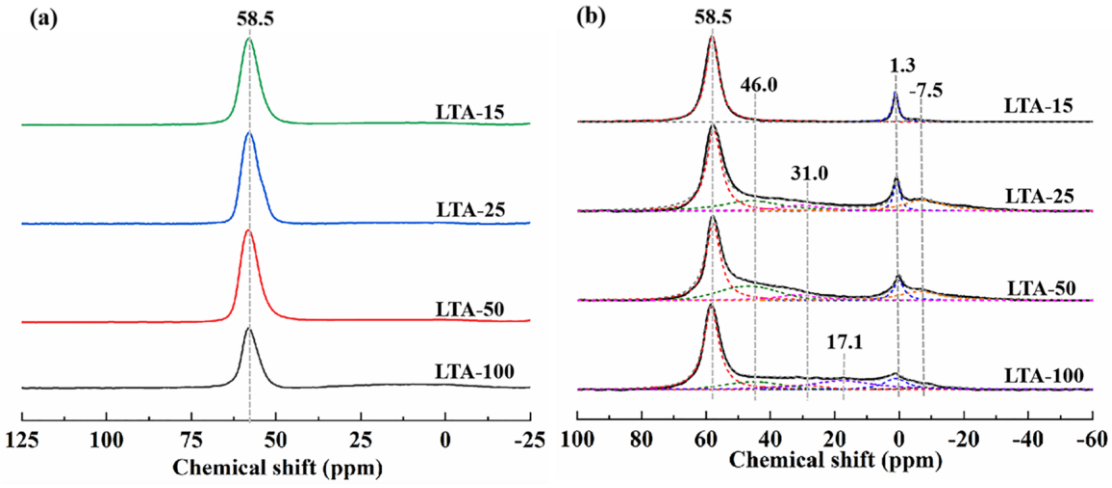

Figure 4. ^{27}Al MAS NMR spectra of the as-synthesized (a) and calcined (b) LTA-*n* zeolites.

In the as-synthesized materials the F^- anions are entrapped in the smallest cage ([4^6] *d4r*) of **LTA** structure. It has several functions, such as compensating the positive

charge introduced by SDA cations in the neighboring big cages and as templets for *d4r*-units. The ^{19}F MAS NMR spectra in Figure 5a show a main resonance at -38 ppm corresponding F^- ions in *d4r*-cages.[7, 30, 31] Large number of *d4r* in **LTA** is the main reason for the difficult synthesis of high- and pure-silica counterparts. Another band at -122 ppm indicates that F^- ions also exist in the big *lta*-cage, compensating SDA cations.[20] F^- ions work to correct the structural tensions, together with the SDAs in the *sod*- and *lta*-cages. In addition, the spectra of as-synthesized samples present an isotropic band at -149 ppm, which could be ascribed to the multiple environments of F^- ions connected with the framework Si sites, i.e., F_x–Si(–OSi)$_3$.[32] They take a significant portion of the total F^- amount, and should not be imputed to unreacted silica or alumina precursors. Rather, connectivity defects, either related to the *d4r*-unit or not, exist already in the as-synthesized materials and are capped by F^- ions. However, after calcination, F^- ions in *d4r*- are removed (Figure 5b). Some extra-framework SiF_4 at -161 ppm is observed. And, new F^- ions environments a small amount of F_y–Si(–OSi)$_3$ at -108 ppm appear, where $y < x$.[33, 34] To be noticed, the total amount of F^- in the calcined materials is low. These remaining species are just barely observed above the noise.

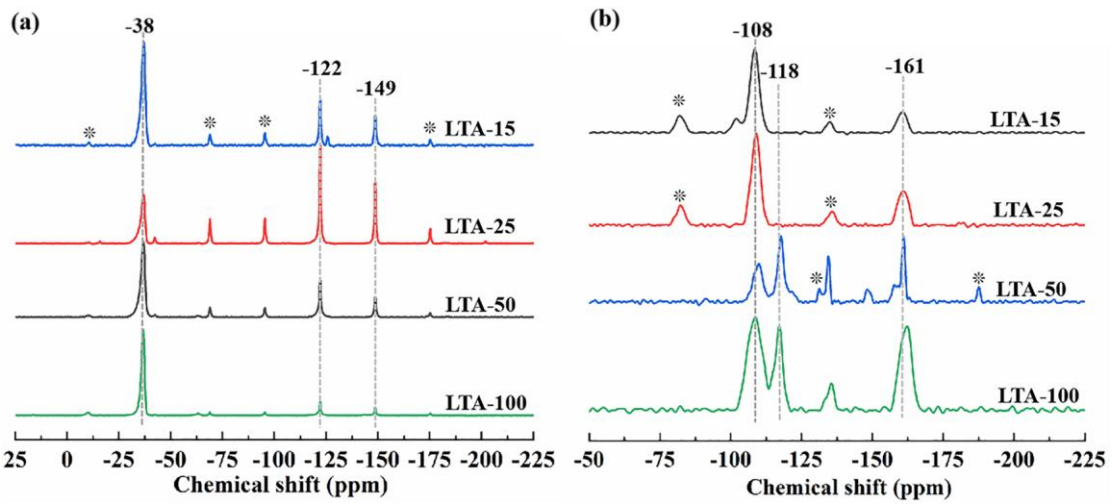

Figure 5. ^{19}F MAS NMR spectra of the as-synthesized (a) and calcined (b) LTA-*n* zeolites. Spinning sidebands are marked with an asterisk (*).

3.3 Acidity test and catalytic performance

3.3.1 Acidity of calcined LTA-*n* zeolites

Figure 6 shows NH_3-TPD profiles of the calcined materials. The desorption of NH_3 commenced at approximately 100 °C and ended at over 550 °C, deriving from those bound to BAS from bridging or terminal hydroxyl (-OH) groups and LAS from the extraframework Al metal sites.[35] For calcined LTA-*n* materials, two NH_3-TPD bands centered at approximately 170 and 400-430 ^{o}C imply weak and medium-strength acid sites. The total amounts of desorbed NH_3 increase with increasing Al contents (Table 3).[36] It is also noticeable that a gradual shift of the NH_3-desorption peak of the medium acid sites from a lower to a higher temperature, suggesting an increase in acidic strength of medium acid sites at elevated Al ratio.

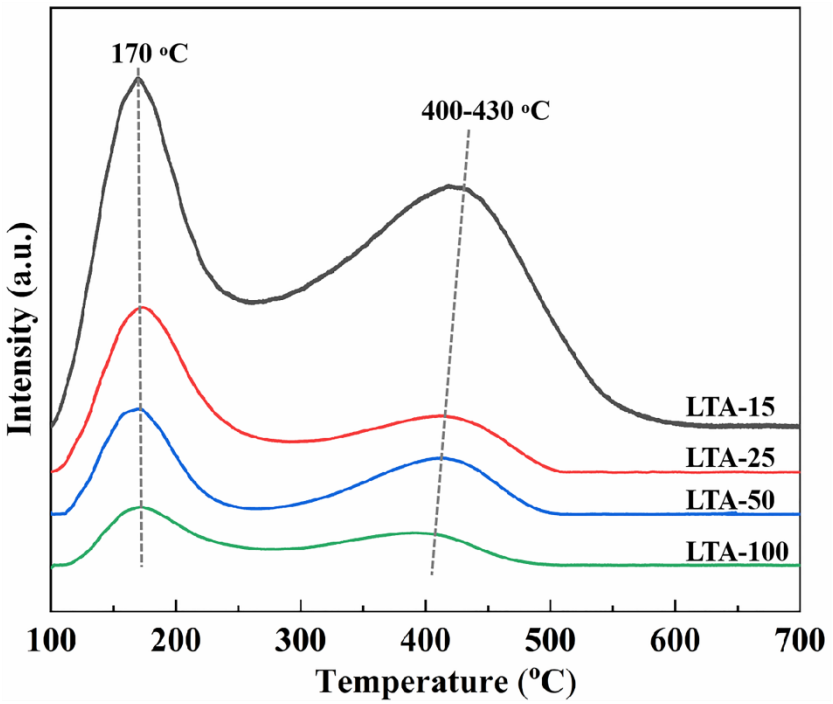

Figure 6. NH_3-TPD profiles of the calcined LTA-*n* zeolites.

Table 3. The acidic properties of LTA-*n* zeolites.

Samples	Total acid sites[a] (μmol/g)	LAS[b] (μmol/g)	BAS[b] (μmol/g)			LAS/BAS
			Moderate	Weak	Total	
LTA-100	178	30	50	98	148	0.20
LTA-50	301	96	100	105	205	0.47
LTA-25	497	163	157	177	334	0.49
LTA-15	629	205	201	223	424	0.48

[a] The total acid site was determined by the NH_3-TPD.

[b] The densities of Brønsted acid sites (BAS) and Lewis acid sites (LAS) were obtained at 150 °C by the FTIR of CD_3CN desorption.

Figure S4 displays the FTIR spectra of the calcined materials activated at 450 °C for 2 h in vacuum. The studied range between 3850 and 3350 cm^{-1} corresponds to the

stretching vibrations of hydroxyl groups. The distribution of different peaks varies between samples. The intense band centered at about 3620 cm^{-1} is due to the hydroxyl group bridging Si and Al (Si-OH-Al), i.e., the Brønsted acid sites (BAS).[37, 38] The band intensifies with increasing framework Al contents. The band at 3564 cm^{-1} is assigned to bridging hydroxyl group whose oxygen atoms are crystallographically different from those of already known Brønsted acid sites.[29, 39] It was reported LTA zeolite contains 3 possible Si-OH-Al Brønsted acid sites, distinguished by the type of oxygen (O1, O2, O3).The Si-O1H-Al and Si-O2H-Al groups are lies in a single 8-ring window shared between two *lta* cages. Si-O3H-Al groups are located in a single 6-ring window shared between *lta* and *sod* cages. O1H and O3H point toward the large cavity whereas O2H vibrates close to the small cavity.[29, 39] The bands at 3676 and 3730 cm^{-1} are isolated silanols at the internal and external surfaces, respectively.[37, 40] Internal isolated silanols are at connectivity defects. Another barely observable peak at 3786 cm^{-1} is associated with Al-OH of extra-framework Al species.[37, 40] The bands ascribed to silanols and extra-framework Al were more intense on low Si/Al ratio samples (LTA-15 and LTA-25).

Figure 7 depicts normalized FTIR spectra of LTA-*n* zeolite samples with CD_3CN desorbed at 150 ^oC. There are three stretching modes of υ (C≡N) in the range of 2240–2350 cm^{-1}. The band at 2330-2310 is attributed to the interaction of CD_3CN with LAS due to extra-framework oxo-aluminium species. The band at 2296 cm^{-1} is the bridging -OH groups (Si-OH-Al), i.e., the BAS. Another band at 2287 cm^{-1} reflects the weak BAS of terminal Si-OH groups and internal -OH groups of Si-OH and/or

Al-OH.[41] The absence of the peak at 2264 cm^{-1} proves that physisorbed D3-acetonitrile has been completely removed by evacuation.[42] Quantitative evaluations of the acid sites on the LTA-*n* materials by FTIR and the NH_3-TPD profiles respecting the densities of LAS, BAS, and total acid sites, are summarized in Table 3. The ratios of BAS and LAS were calculated from the area of the band centered at 2280-2300 and 2310-2330 cm^{-1}, respectively.[43]

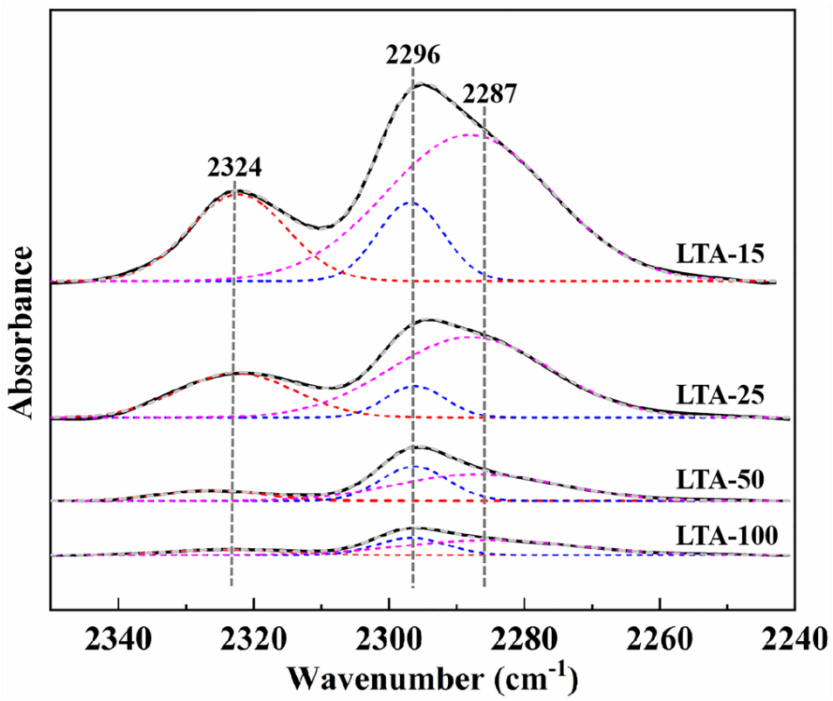

Figure 7. FTIR spectra of the calcined LTA-*n* zeolites using CD_3CN as a probe molecule.

This result suggests that the total number of acid sites, both BAS and LAS, increase with Al contents. However, due to the dealumination during calcination, LAS and BAS numbers do not raise parallel with the Al contents. The lower Si/Al ratio versions also contain higher portions of LAS. The calcined LTA-100 has LAS/BAS = 0.2. But the values for calcined LTA-25 and LTA-15 are ca. 0.5. These materials contain high

portions of Lewis sites, than most other zeolites of similar Si/Al ratios.

3.3.2 Catalytic performance and catalysts deactivation

In MTO tests, methanol conversions over calcined LTA-*n* catalysts as a function of time on stream (TOS) at 400 °C was plotted in Figure 8. The lifetimes of the catalysts were defined by the breakthrough times of methanol. Remarkably the total amount of converted methanol correlated with the amount of moderate-strength BAS as shown in Figure 8 (insert). LTA-100 with the least moderate-strength BAS (50 μmol/g) exhibited the shortest catalyst lifetime of only 96 min. Increasing the Al content prolonged the catalyst lifetime to 180 min for LTA-15 with 201 μmol/g moderate-strength BAS. In addition, enhanced BAS strength could be another reason for prolonged catalyst lifetimes.[38]

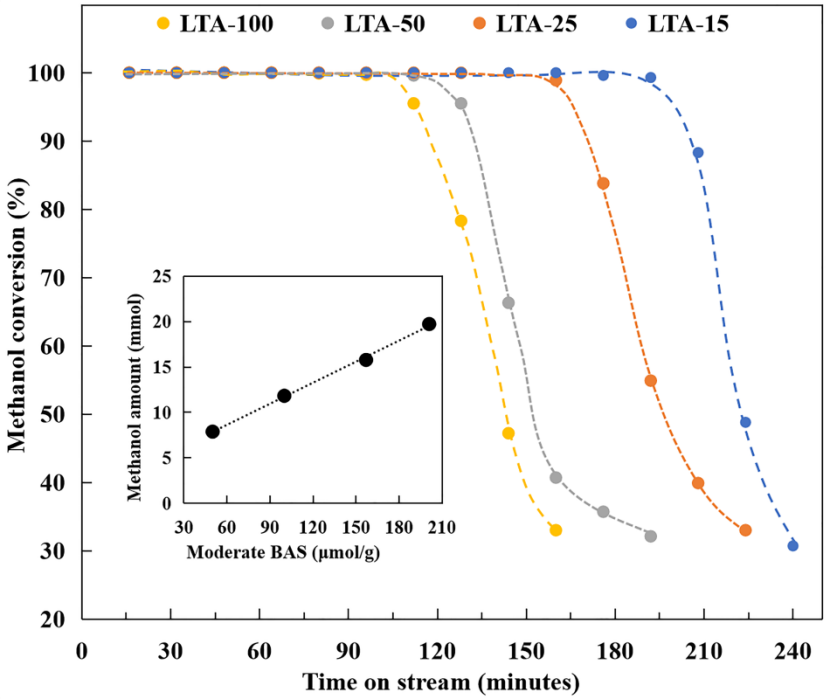

Figure 8. Methanol conversion versus time on stream over calcined LTA-*n* zeolites.

Insert: Consumed methanol amount before the catalysts start to deactivate *versus* the density of moderate BAS. (T= 400 °C, *p*=0.1 MPa, WHSV=2 h^{-1}).

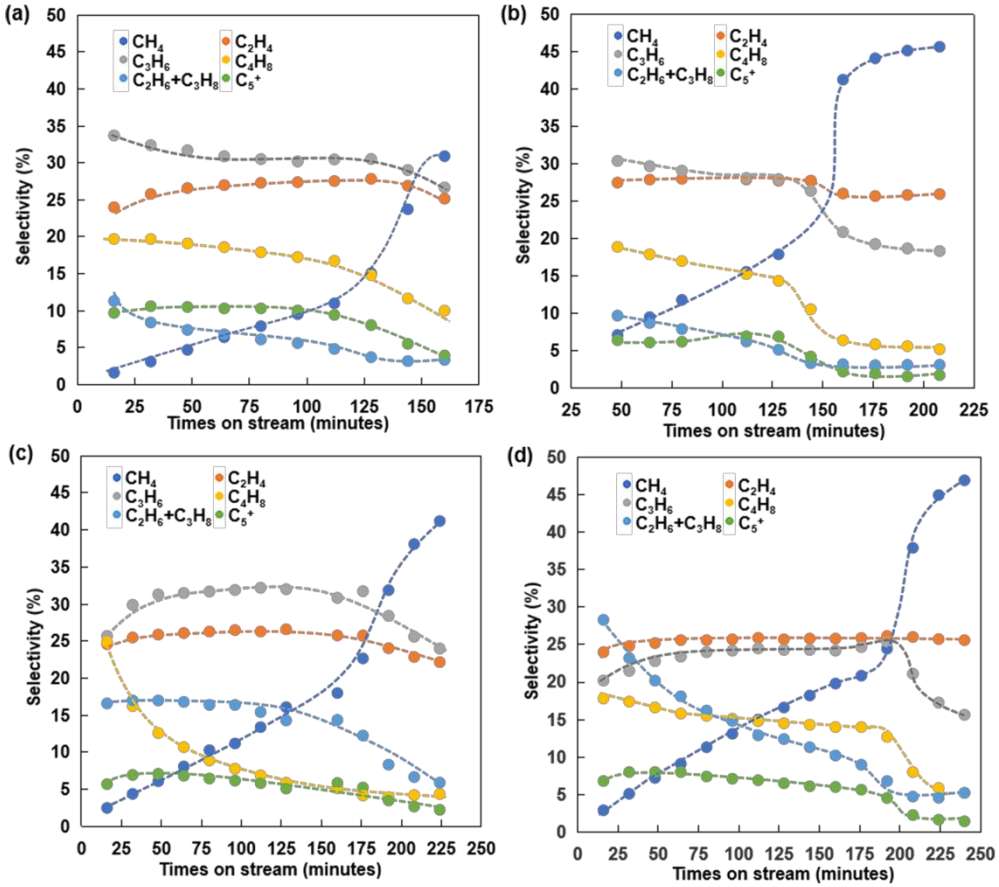

Figure 9. Products selectivity during MTO reaction over calcined LTA-*n* zeolites *versus* time on stream: (a) LTA-100, (b) LTA-50, (c) LTA-25, and (d) LTA-15 (T= 400°C, p=0.1 MPa, WHSV=2 h^{-1}).

Products distribution in MTO reaction over LTA-*n* catalysts was studied as a function of Si/Al ratios (Figure 9 and 10). Notably, all calcined LTA-*n* catalysts with different acidity were highly selective to ethylene and propylene within the 50-60% range in MTO reaction. The selectivity toward ethylene (C_2H_4) over all catalysts was about 25%, which is independent from the zeolite acidity. However, the ethylene/propylene

ratio (C_2H_4/C_3H_6) varied widely with the Si/Al ratio.

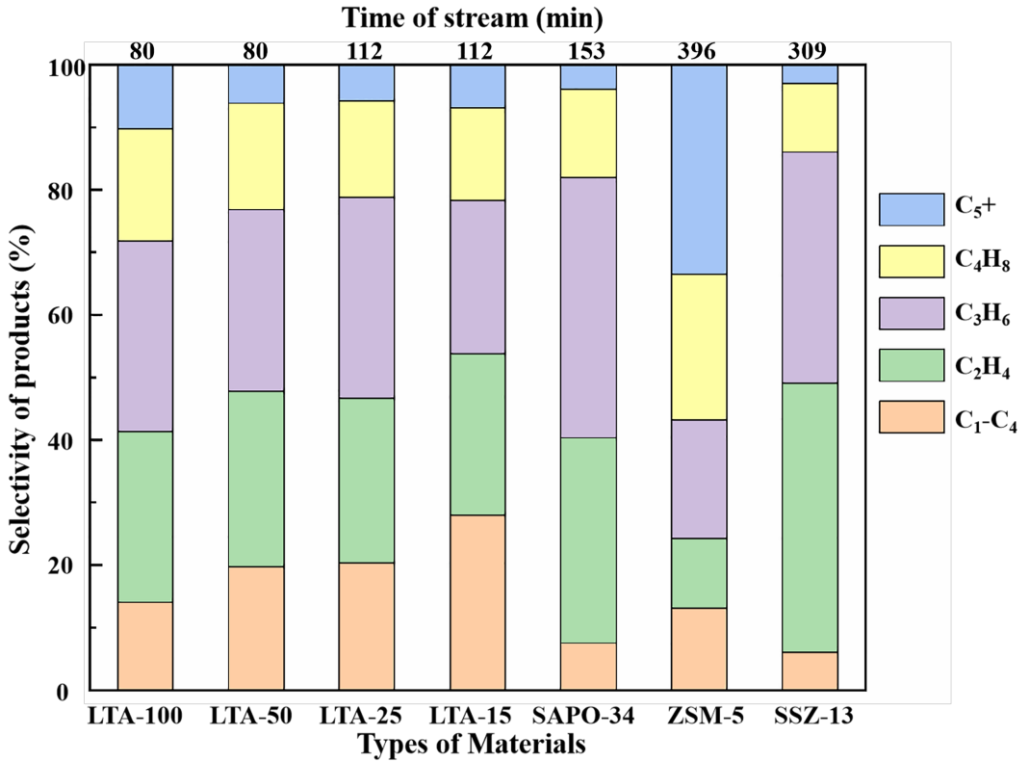

Figure 10. Product selectivity in the MTO reaction of LTA-*n* series compared with other types of zeolites. C_1-C_4 includes fully saturated hydrocarbons containing 1−4 carbon atoms and C_4H_8 includes all isomeric butenes (but-1-ene, (Z)-but-2-ene, (E)-but-2-ene, and 2-methylpropene). The upper of this Figure gives the reaction time for discussed activity over the different materials.

Different from other samples, calcined LTA-15 displayed a higher C_2H_4/C_3H_6 ratio (>1), which could be due to the higher acid strength in LTA-15 as shown in Figure 6. This could be because that a higher acid strength favors the formation of C_2H_4, because C_3H_8 diffuses slower and thus faces a higher probability of being cracked at stronger BAS.[44-45] On the other hand, the selectivity toward light alkane (e.g., C_2H_6 and C_3H_8) over LTA-*n* catalysts increased with decreasing Si/Al ratio. Heavier

hydrocarbons and aromatics (C_5^+) contribute to the rest of the products. Methane became significant when the catalysts are deactivating and becomes dominant when methanol breaks through.

3.4 Comparisons between different zeolites with various frameworks

The acidity and catalytic activity of calcined LTA-25 were compared to **CHA**-type (SSZ-13, SAPO-34) and **MFI**-type (ZSM-5) zeolites, which are intensively studied for MTO.[8, 46-48] The pore structures and acidity of these materials are given in Table S4 and S5. The SEM pictures, NH_3-TPD results, and full reaction profiles are given in Figures S5-S8 and Figure 10. The numbers of moderate-strength acid sites of these catalysts are in the order of LTA-25 < ZSM-5 < SSZ-13 < SAPO-34. The reaction profiles for each zeolite are different, and data are shown in Figure 10 for comparison at 100% methanol conversion. As expected, SSZ-13 and SAPO-34 showed high selectivity to C_2H_4 and C_3H_6 of 80 % and 74.4 %, respectively. ZSM-5, with a 10MR channel system, gave a lower selectivity to light olefins but higher selectivity to C_4H_8 (23.3 %) and C_5^+ products (33.5 %) compared to the 8MR zeolites. LTA-25 zeolite was less selective to C_2H_4 and C_3H_6, but more selective to C_4H_8 than **CHA**-type zeolites. SSZ-13, SAPO-34, and ZSM-5 had significantly longer lifetimes than LTA-25 (Figure S7). The fastest deactivation over **LTA**-type zeolites is caused by a combination of several factors, such as the strength of BAS, and the significant portion of LAS. The pore geometry may also be significantly involved in deactivation, too. **LTA** zeolite has a cage with a bigger diameter than **CHA**, but with a smaller volume.

Also, **LTA** has isometric cage, while **CHA** is elliptical. The intermediate hydrocarbon-pool species can grow larger in **LTA** than in **CHA** zeolite regarding its diffusion diameter and entrapped there.[49] Although the 8MR window of **LTA** zeolite is slightly larger, the harder cokes inside the cage still hardly leave. Only being cracked deeply to methane, free movement is allowed. Therefore, LTA-*n* zeolites have growing methane selectivity along with time on stream.

4. Conclusions

The high-silica materials with Si/Al ratios of ca. 15 to ∞ have been synthesized. The experimental results show that the large number of *d4r* in **LTA** that is the preferred location of Al atoms is the main reason for the difficult synthesis of high and all-silica counterparts. The synthesis of high silica zeolite A is possible by employing two SDAs, imidazolium and tetramethylammonium that exhibit strong interactions with the zeolite framework. Thus the framework of as-synthesized materials is contracted inward, distorted, and possesses point-defects. The complete removal of SDAs by calcination in air is only possible at temperatures above 700 °C. After calcination, the retained framework structure becomes relaxed and more ordered. However, framework dealumination has occurred that resulted in connectivity defects and a high portion of Lewis acid sites. All these factors, i.e., the unique porous structure, defective framework, and the unusual combination of Brønsted and Lewis acidity, make the material behave in the MTO reaction differently from **CHA**-type and **MFI**-type catalysts. The systematic study on the **LTA** high-silica zeolites acidity will

be useful for considering this material for alternative applications.

5. Conflicts of interest

There are no conflicts of interest to declare.

6. Acknowledgments

The ZeoMat Group acknowledges the starting grant provided by QIBEBT, and the support provided by the Shandong Energy Institute (SEI S202107), the Nature Science Foundation of Shandong Province (ZR2022MB053), and Applied Basic Research Fund of Qingdao (E2396101). VV, XY, and PL acknowledge the collaboration under the Sino-French International Research Network (IRN) “Zeolites”.

Reference:

1. Breck, D. W.; Eversole, W. G.; Milton, R. M., New Synthetic Crystalline Zeolites. *Journal of the American Chemical Society* **1956,** *78* (10), 2338-2339.

2. Collins, F.; Rozhkovskaya, A.; Outram, J. G.; Millar, G. J., A Critical Review of Waste Resources, Synthesis, and Applications for Zeolite LTA. *Microporous and Mesoporous Materials* **2020,** *291*.

3. Yue, B.; Liu, S.; Chai, Y.; Wu, G.; Guan, N.; Li, L., Zeolites for separation: Fundamental and application. *Journal of Energy Chemistry* **2022**, 71, 288-303.

4. Global Zeolite 4A Market Status and Prospect. *360 Market:* **2023**.

5. Loewenstein, W., The Distribution of Aluminum in the Tetrahedra of Silicates and Aluminates. *American Mineralogist* **1954,** *39* (1-2), 92-96.

6. Bell, R. G.; Jackson, R. A.; Catlow, C. R. A., Löwenstein's Rule in Zeolite A: A Computational Study. *Zeolites* **1992,** *12* (7), 870-871.

7. Boal, B. W.; Schmidt, J. E.; Deimund, M. A.; Deem, M. W.; Henling, L. M.; Brand, S. K.; Zones, S. I.; Davis, M. E., Facile Synthesis and Catalysis of Pure-Silica and Heteroatom LTA. *Chemistry of Materials* **2015,** *27* (22), 7774-7779.

8. Zhong, J.; Han, J.; Wei, Y.; Tian, P.; Guo, X.; Song, C.; Liu, Z., Recent Advances of the Nano-Hierarchical SAPO-34 in the Methanol-to-Olefin (MTO) Reaction and Other Applications. *Catalysis Science & Technology* **2017,** *7* (21), 4905-4923.

9. Derouane, E. G.; Vedrine, J. C.; Ramos Pinto, R.; Borges, P. M.; Costa, L.; Lemos, M. A. N. D. A.; Lemos, F.; Ramoa Ribeiro, F., The Acidity of Zeolites: Concepts, Measurements and Relation to Catalysis: A Review on Experimental and Theoretical Methods for the Study of Zeolite Acidity. *Catalysis Reviews-Science and Engineering* **2013,** *55* (4), 454-515.

10. Vogt, E. T. C.; Weckhuysen, B. M., Fluid Catalytic Cracking: Recent Developments on the Grand Old Lady of Zeolite Catalysis. *Chemical Society Reviews* **2015,** *44* (20), 7342-7370.

11. Li, H.; Yang, S.; Riisager, A.; Pandey, A.; Sangwan, R. S.; Saravanamurugan, S.; Luque, R., Zeolite and Zeotype-Catalysed Transformations of Biofuranic Compounds.

Green Chemistry **2016,** *18* (21), 5701-5735.

12. Weitkamp, J., Zeolites and Catalysis. *Solid State Ionics* **2000,** *131* (1-2), 175-188.

13. Barrer, R. M.; Denny, P. J., 201. Hydrothermal Chemistry of the Silicates. Part Ix. Nitrogenous Aluminosilicates. *Journal of the Chemical Society (Resumed)* **1961,** (0), 971-982.

14. Kerr, G. T.; Kokotail.Gt, Sodium Zeolite ZK-4, A New Synthetic Crystalline Aluminosilicate. *Journal of the American Chemical Society* **1961,** *83* (22), 4675-&.

15. Kerr, G. T., Chemistry of Crystalline Aluminosilicates. II. The Synthesis and Properties of Zeolite ZK-4. *Inorganic Chemistry* **1966,** *5* (9), 1537-1539.

16. Kuehl, G. H., High-Silica Analogs of Zeolite a Containing Intercalated Phosphate. *Inorganic Chemistry* **1971,** *10* (11), 2488-2495.

17. Lewis, G. J.; Miller, M. A.; Moscoso, J. G.; Wilson, B. A.; Knight, L. M.; Wilson, S. T., Experimental Charge Density Matching Approach to Zeolite Synthesis. In *Recent Advances in the Science and Technology of Zeolites and Related Materials, Pts A - C*, VanSteen, E.; Claeys, M.; Callanan, L. H., Eds. **2004**; Vol. 154, pp 364-372.

18. Park, J. W.; Lee, J. Y.; Kim, K. S.; Hong, S. B.; Seo, G., Effects of Cage Shape and Size of 8-Membered Ring Molecular Sieves on Their Deactivation in Methanol-to-Olefin (MTO) Reactions. *Applied Catalysis A-General* **2008,** *339* (1), 36-44.

19. Corma, A.; Rey, F.; Rius, J.; Sabater, M. J.; Valencia, S., Supramolecular Self-Assembled Molecules as Organic Directing Agent for Synthesis of Zeolites. *Nature* **2004,** *431* (7006), 287-290.

20. Bouizi, Y.; Paillaud, J.-L.; Simon, L.; Valtchev, V., Seeded Synthesis of Very High Silica Zeolite A. *Chemistry of Materials* **2007,** *19* (4), 652-654.

21. Jo, D.; Ryu, T.; Park, G. T.; Kim, P. S.; Kim, C. H.; Nam, I.-S.; Hong, S. B., Synthesis of High-Silica **LTA** and **UFI** Zeolites and NH_3-SCR Performance of Their Copper-Exchanged Form. *ACS Catalysis* **2016,** *6* (4), 2443-2447.

22. Baerlocher, C.; Meier, W. M., Synthese Und Kristallstruktur Von Tetramethylammonium-Sodalith. *Helvetica Chimica Acta* **1969,** *52* (7), 1853-1860.

23. Kresnawahjuesa, O.; Olson, D. H.; Gorte, R. J.; Kühl, G. H., Removal of Tetramethylammonium Cations from Zeolites. *Microporous and Mesoporous Materials* **2002,** *51* (3), 175-188.

24. Lakiss, L.; Kouvatas, C.; Gilson, J.-P.; Aleksandrov, H. A.; Vayssilov, G. N.; Nesterenko, N.; Mintova, S.; Valtchev, V., Unlocking the Potential of Hidden Sites in Faujasite: New Insights in a Proton Transfer Mechanism. *Angewandte Chemie International Edition* **2021,** *60* (51), 26702-26709.

25. Palcic, A.; Ordomsky, V. V.; Qin, Z.; Georgieva, V.; Valtchev, V., Tuning Zeolite Properties for a Highly Efficient Synthesis of Propylene from Methanol. *Chemistry-A European Journal* **2018,** *24* (50), 13136-13149.

26. Klinowski, J., Solid-State NMR-Studies of Molecular-Sieve Catalysts. *Chemical Reviews* **1991,** *91* (7), 1459-1479.

27. Chen, T. H.; Wouters, B. H.; Grobet, P. J., Aluminium Coordinations in Zeolite Mordenite by Al-27 Multiple Quantum Mas NMR Spectroscopy. *European Journal of Inorganic Chemistry* **2000,** (2), 281-285.

28. Jiao, J.; Kanellopoulos, J.; Wang, W.; Ray, S. S.; Foerster, H.; Freude, D.; Hunger, M., Characterization of Framework and Extra-Framework Aluminum Species in Non-Hydrated Zeolites Y by Al-27 Spin-Echo, High-Speed MAS, and MQ MAS NMR Spectroscopy at B-0=9.4 to 17.6 T. *Physical Chemistry Chemical Physics* **2005,** *7* (17), 3221-3226.

29. Ahn, S. H.; Wang, Q.; Wang, Y.; Chu, Y.; Deng, F.; Hong, S. B., Identifying Crystallographically Different Si-OH-Al Brønsted Acid Sites in LTA Zeolites. *Angewandte Chemie-International Edition* **2022**, 61 (24), e202203603.

30. Mafra, L.; Vidal-Moya, J. A.; Blasco, T., Chapter Four-Structural Characterization of Zeolites by Advanced Solid State NMR Spectroscopic Methods. In *Annual Reports on NMR Spectroscopy*, Webb, G. A., Ed. Academic Press: **2012**; Vol. 77, pp 259-351.

31. Liu, X.; Chu, Y.; Wang, Q.; Wang, W.; Wang, C.; Xu, J.; Deng, F., Identification of Double Four-Ring Units in Germanosilicate ITQ-13 Zeolite by Solid-State NMR Spectroscopy. *Solid State Nuclear Magnetic Resonance* **2017,** *87*, 1-9.

32.Shi, D.; Fu, G.; Omran, A.; Haw, K.-G.; Zhu, L.; Ding, R.; Lang, Q.; Wang, S.; Fang,

Q.; Qiu, S.; Yang, X.; Valtchev, V., Acidic Properties of Al-Rich ZSM-5 Crystallized in Strongly Acidic Fluoride Medium. *Microporous and Mesoporous Materials* **2022**, 112332.

33. Fu, G.; Dib, E.; Lang, Q.; Zhao, H.; Wang, S.; Ding, R.; Yang, X.; Valtchev, V., Acidic Medium Synthesis of Zeolites - an Avenue to Control the Structure-Directing Power of Organic Templates. *Dalton Transactions* **2022,** *51* (30), 11499-11506.

34. Koller, H.; Wölker, A.; Villaescusa, L. A.; Díaz-Cabañas, M. J.; Valencia, S.; Camblor, M. A., Five-Coordinate Silicon in High-Silica Zeolites. *Journal of the American Chemical Society* **1999,** *121* (14), 3368-3376.

35. Jiang, Y. J.; Huang, J.; Dai, W. L.; Hunger, M., Solid-State Nuclear Magnetic Resonance Investigations of the Nature, Property, and Activity of Acid Sites on Solid Catalysts. *Solid State Nuclear Magnetic Resonance* **2011,** *39* (3-4), 116-141.

36. Xu, H. M.; Wang, Z. C.; Miao, Z. C.; Zhu, Y. X.; Marianov, A.; Wang, L. Z.; Castignolles, P.; Gaborieau, M.; Huang, J.; Jiang, Y. J., Correlation between Acidity and Catalytic Performance of Mesoporous Zirconium Oxophosphate in Phenylglyoxal Conversion. *ACS Sustainable Chemistry & Engineering* **2019,** *7* (9), 8931-8942.

37. Jia, C.; Massiani, P.; Barthomeuf, D., Characterization by Infrared and Nuclear-Magnetic-Resonance Spectroscopies of Calcined Beta-Zeolite. *Journal of the Chemical Society-Faraday Transactions* **1993,** *89* (19), 3659-3665.

38. Holm, M. S.; Svelle, S.; Joensen, F.; Beato, P.; Christensen, C. H.; Bordiga, S.;

Bjorgen, M., Assessing the Acid Properties of Desilicated ZSM-5 by FTIR Using Co and 2,4,6-Trimethylpyridine (Collidine) as Molecular Probes. *Applied Catalysis A-General* **2009,** *356* (1), 23-30.

39. Lemishko, T.; Valencia, S.; Rey, F.; Jimenez-Ruiz, M.; Sastre, G., Inelastic Neutron Scattering Study on the Location of Brønsted Acid Sites in High Silica LTA Zeolite. J*ournal of Physical Chemistry C* **2016**, 120 (43), 24904-24909.

40. Barbera, K.; Bonino, F.; Bordiga, S.; Janssens, T. V. W.; Beato, P., Structure-Deactivation Relationship for ZSM-5 Catalysts Governed by Framework Defects. *Journal of Catalysis* **2011,** *280* (2), 196-205.

41. Dai, W. J.; Ruaux, V.; Deng, X.; Tai, W. S.; Wu, G. J.; Guan, N. J.; Li, L. D.; Valtchev, V., Synthesis and Catalytic Application of Nanorod-Like **FER**-Type Zeolites. *Journal of Materials Chemistry A* **2021,** *9* (44), 24922-24931.

42. Pelmenschikov, A. G.; Vansanten, R. A.; Janchen, J.; Meijer, E., CD_3CN as a Probe of Lewis and Brønsted Acidity of Zeolites. *Journal of Physical Chemistry* **1993,** *97* (42), 11071-11074.

43. Wichterlova, B.; Tvaruzkova, Z.; Sobalik, Z.; Sarv, P., Determination and Properties of Acid Sites in H-Ferrierite - A Comparison of Ferrierite and MFI Structures. *Microporous and Mesoporous Materials* **1998,** *24* (4-6), 223-233.

44.Bleken, F.; Bjorgen, M.; Palumbo, L.; Bordiga, S.; Svelle, S.; Lillerud, K. P.; Olsbye, U., The Effect of Acid Strength on the Conversion of Methanol to Olefins over Acidic

Microporous Catalysts with the **CHA** Topology. *Topics in Catalysis* **2009,** *52* (3), 218-228.

45. Wang, C.; Li, B.; Wang, Y.; Xie, Z., Insight into the topology effect on the diffusion of ethene and propene in zeolites: A molecular dynamics simulation study. *Journal of Energy Chemistry* **2013**, 22 (6), 914-918.

46. Yang, M.; Fan, D.; Wei, Y.; Tian, P.; Liu, Z., Recent Progress in Methanol-to-Olefins (MTO) Catalysts. *Advanced Materials* **2019**, 31 (50).

47. Fu, T.; Chang, J.; Shao, J.; Li, Z., Fabrication of a nano-sized ZSM-5 zeolite with intercrystalline mesopores for conversion of methanol to gasoline. *Journal of Energy Chemistry* **2017**, 26 (1), 139-146.

48. Tian, H.; Zhang, Z.; Chang, H.; Ma, X., Catalytic performance of imidazole modified HZSM-5 for methanol to aromatics reaction. *Journal of Energy Chemistry* **2017**, 26 (3), 574-583.

49. Tian, P.; Wei, Y.; Ye, M.; Liu, Z., Methanol to Olefins (MTO): From Fundamentals to Commercialization. *ACS Catalysis* **2015,** *5* (3), 1922-1938.